Group Shape Effects on the Lateral Capacity of Pile Groups in Undrained Soil

Alexander W. Swallow and Brian B. Sheil

Alexander W. Swallow

Department of Engineering Science, University of Oxford, Parks Road, Oxford OX1 3PJ, UK.

Email: awswallow@outlook.com

Brian B. Sheil

Department of Engineering Science, University of Oxford, Parks Road, Oxford OX1 3PJ, UK.

Email: brian.sheil@eng.ox.ac.uk

ORCID: 0000-0002-1462-1401

ABSTRACT

In this paper, the lateral limiting pressure on rectangular pile groups in undrained soil is explored using two−dimensional finite element modelling. The primary aim of the study is to assess the influence of pile group shape effects on the soil limiting pressured offered by the deep 'flow-around' failure mechanism, and associated soil failure mechanisms, considering both a small (four piles) and large (36 piles) group. Additional parameters considered in the modelling include pile spacing and pile-soil interface roughness. The finite element results show that group shape has a significant influence on the behaviour of closely spaced pile groups. In particular, the number of piles parallel to the direction of loading is shown to dominate the lateral bearing capacity factor such that significant increases in capacity efficiency can be achieved by slight modifications to the group shape for a given number of piles. The load-sharing across the group, traditionally defined using *p*-multipliers, was also shown to be highly non-uniform and dependent on group size, pile-soil roughness and group geometry in addition to the pile spacing. The finite element output is presented in the form of design charts for the determination of group *p*-multipliers whereas a library of existing design solutions is presented for the calculation of the overall group response.

INTRODUCTION

Pile foundations are frequently adopted to support structures founded in areas where unfavourable ground conditions prevail and are often the only feasible solution for supporting large structures such as high-rise buildings, bridge piers and wind turbines. These foundations are typically required to resist significant lateral loads from wind, wave or current actions on the superstructure and/or the foundation itself. In recent years, the focus of pile design has shifted towards serviceability limit state resulting in the application of non−linear frameworks to pile group analysis (Sheil et al. 2018). Within a non−linear framework, pile settlement is no longer uncoupled from the ultimate capacity and therefore an accurate capacity estimation remains an essential underpinning element of formal pile design calculations (Sheil and McCabe 2014, 2017).

The response of single piles embedded in undrained soil to lateral loads has been researched extensively in the literature (e.g. Matlock 1970; Brown et al. 1988; Brown and Shie, 1991; Murff and Hamilton, 1993; Yang and Jeremic, 2002). Murff and Hamilton (1993) used upper bound plasticity theory to explore the variation of the ultimate soil resistance acting on a laterally loaded single pile with depth. Those authors noted that the ultimate soil resistance eventually reached a limiting value at a 'critical depth'. This limiting value corresponds to a plane-strain 'flow-around' failure mechanism which depends exclusively on the pile−soil adhesion factor, α.

Previous literature has typically extended the analysis of laterally loaded single piles to pile groups using '*p*-multipliers' to account for the reduction in soil resistance arising from pile interaction effects. Brown et al. (1988) represents one of the earliest studies to propose the use of *p*-multipliers to account for non-uniform load sharing within the group, derived from full-scale tests on a square nine-pile group in sand. Rollins et al. (2006) proposed the use of different *p*-multipliers depending on the pile row within the group where 'leading rows' were assigned a greater *p*-multiplier compared to 'trailing rows'. Results from centrifuge model testing have shown that for a given pile row in a group, central and outer piles experience different loads (Ilyas et al. 2004). This suggests that the application of constant *p*-multipliers to whole rows (e.g. Rollins et al. (2006)) may not always be appropriate. From model tests on 1×2, 2×2, and 1×4 pile groups, Chandrasekaran et

al. (2010) reported a significant influence of group shape and size on *p*-multipliers within the group noting that the spacing of piles perpendicular, as well as parallel, to the direction of loading should be considered in design. Comodromos and Pitilakis (2005) and Comodromos and Papadopoulou (2012, 2013) used three-dimensional numerical modelling to inform the development of new design methods to describe the load-displacement response of a horizontally loaded pile group. More recently, Fayyazi et al. (2014) highlighted the limitations of existing prescriptive design approaches where poor predictions were obtained for *p*-multipliers for square groups of 9, 16, 25 and 36 piles.

It is therefore widely accepted in the literature that the placement of piles in closely spaced groups reduces bearing capacity compared to equivalent single pile values (McCabe and Sheil 2015). However, while rigorous solutions for the limiting pressure at depth are now available for single piles (Randolph and Houlsby, 1984; Murff et al. 1989; Martin and Randolph, 2006), current understanding of how this limiting pressure applies to pile groups is much less advanced (Georgiadis et al. 2013b). Using three-dimensional finite element (FE) modelling, Georgiadis (2014) reported that group effects on the ultimate soil pressure acting on a pile row were depth-dependent: pile interaction was negligible close to the soil surface and tended to a higher limiting value at greater depths. Georgiadis et al. (2013a,2013b), Zhao et al. (2017a) and Zhao et al. (2017b) used two-dimensional FE modelling to derive expressions for the ultimate bearing capacity for a group of two, three and four piles respectively, considering pile spacing, pile-soil adhesion and load direction. More recently, Sheil (2020) used two-dimensional FE to develop closed-form equations for the determination of the limiting pressure acting on square groups of 4 to 25 piles.

Accurate estimation of the resistance offered by the deep ‘flow-around’ soil failure mechanism is essential for future development of more rigorous design solutions for laterally loaded pile groups. However, the literature lacks rigorous generalised solutions. This paper addresses this shortcoming using two−dimensional small-strain finite element modelling to assess the influence of group shape on the behaviour of laterally loaded pile groups considering both a small (four piles) and large (36 piles) group. Additional parameters considered in the modelling include pile spacing and pile-soil interface roughness. The main contributions of this paper are as follows: (i) it assesses the influence of group shape on the soil limiting pressure, load sharing and soil failure

mechanisms of both small and large pile groups, (ii) it identifies the variation of *p*-multipliers within the group and presents design charts for their determination as a function of group shape and size, pile spacing and pile roughness, (iii) through comparisons to existing prescriptive design methods, the numerical output is used to isolate the contribution of the deep failure mechanism on the *p*-multiplier determination, and (iv) by establishing the dominance of pile rows on the group behaviour, it presents a library of existing design methods for the determination of the undrained bearing capacity factor for a wide range of group shapes and sizes.

FINITE ELEMENT MODEL

Problem definition

Figure 1 defines the problem considered in this paper. Plane strain conditions are adopted to study the resistance offered by the deep 'flow-around' soil failure mechanism. Rectangular groups of piles are modelled using a pile diameter, D, of 1 m (fixed) and pile−to−pile spacing, s (varied). Two group sizes, n, are considered: (a) a 'small' group of n = 4 piles and (b) a 'large' group of n = 36 piles (chosen for its high number of integer factors). The pile/soil parameters considered in the modelling are summarised in Tables 1 and 2 for the small and large group, respectively. The piles are always displaced in the y direction by the same prescribed displacement, δ, to simulate rigid pile cap conditions; a value of $\delta = 0.5D$ was adopted in these analyses to ensure pile failure was achieved. For a given group size, analysis of all possible rectangular group shapes results in pairs of identical groups loaded in two mutually orthogonal directions (e.g. 1×4 and 4×1). In such a case, the results of Zhao et al. (2017b) suggest that alternative loading directions (i.e. not aligned with either the x or y direction in Fig. 1) yield intermediate estimates of the ultimate capacity. Therefore, the results presented henceforth provide upper and lower bound capacity estimates for a given group shape.

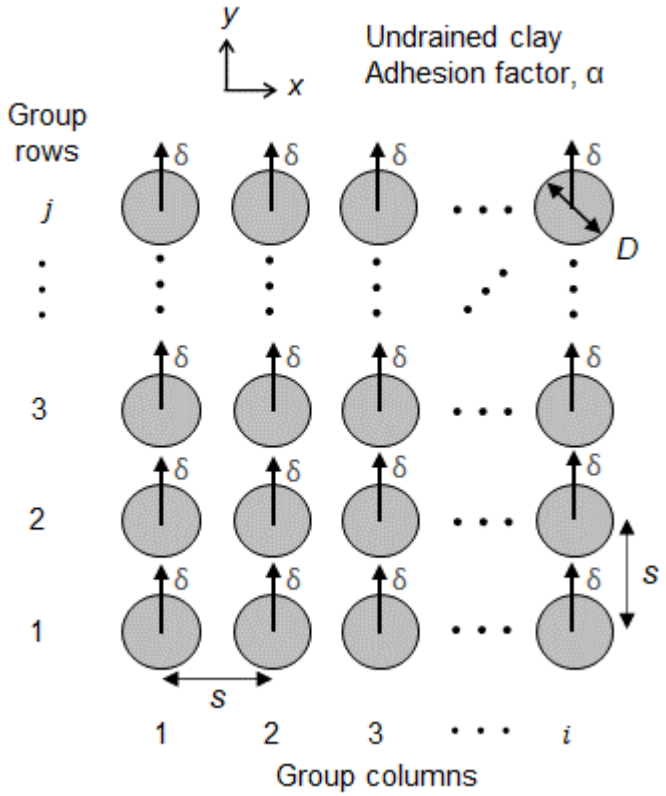

Fig. 1 Definition of an *i*×*j* pile group where the piles are always loaded in the *y* direction.

Table 1 Small group (*n* = 4) analyses.

Parameter	**Value(s)**
Pile-soil adhesion factor, *α*	0, 1
Group Geometries, *ixj*	1×4, 2×2, 4×1
Normalised pile spacing, *s/D*	1.05, 1.25, 1.5, 2, 2.5, 3, 3.5, 4, 4.5, 5, 5.5, 6,

Table 2 Large group (*n* = 36) analyses.

Parameter	**Value(s)**
Pile-soil adhesion factor, *α*	0, 1
Group Geometries, *ixj*	1×36, 2×18, 3×12, 4×9, 6×6, 9×4, 12×3, 18×2, 36×1
Normalised pile spacing, *s/D*	2, 4

Material parameters

The soil was modelled as a weightless elastic perfectly plastic Tresca material with an undrained shear strength, s_u = 100 kPa, Poisson's ratio, v_u = 0.495, and Young's modulus, $E_u = 500 \cdot s_u$. The piles were modelled as a linear elastic steel pipe with a Young's modulus, $E_p = 2.1 \times 10^6 \cdot s_u$ and Poisson's ratio, v_p, of 0.1. A wall thickness of 50 mm was adopted to ensure the pile effectively

behaved as a rigid body during loading. he pile-soil interface was modelled using interface elements obeying elastic perfectly plastic Tresca behaviour with an undrained shear strength of αs_u where α = 1 and 0 correspond to a fully rough and fully smooth pile respectively. A shear stiffness of ~1 MPa and normal stiffness of ~100 MPa were assigned to the interface to approximate rigid−plastic interface behaviour. To study the flow-around failure mechanism, full tension interface conditions were imposed at the pile-soil interface to prevent the development of gapping in the modelling (Randolph and Houlsby 1984; Georgiadis et al. 2013a, 2013b).

Finite element mesh

The small-strain FE analyses were completed using Plaxis 2D 2019. The soil was modelled using fourth−order, 15−node triangular elements while the steel pipe pile was modelled using 5−node beam elements. For each analysis, distances to lateral boundaries varied depending on the group size and spacing and were adjusted such that the soil failure mechanisms were comfortably contained within the computational domain. However, the same mesh density close to the piles was preserved in all analyses. All boundaries were restricted from movement normal to their respective surface. Exemplar meshes are shown in Fig. 2 for a single pile and pile group (a 6×6 group is shown for illustrative purposes) where geometrical and loading symmetry was exploited to reduce the number of elements required.

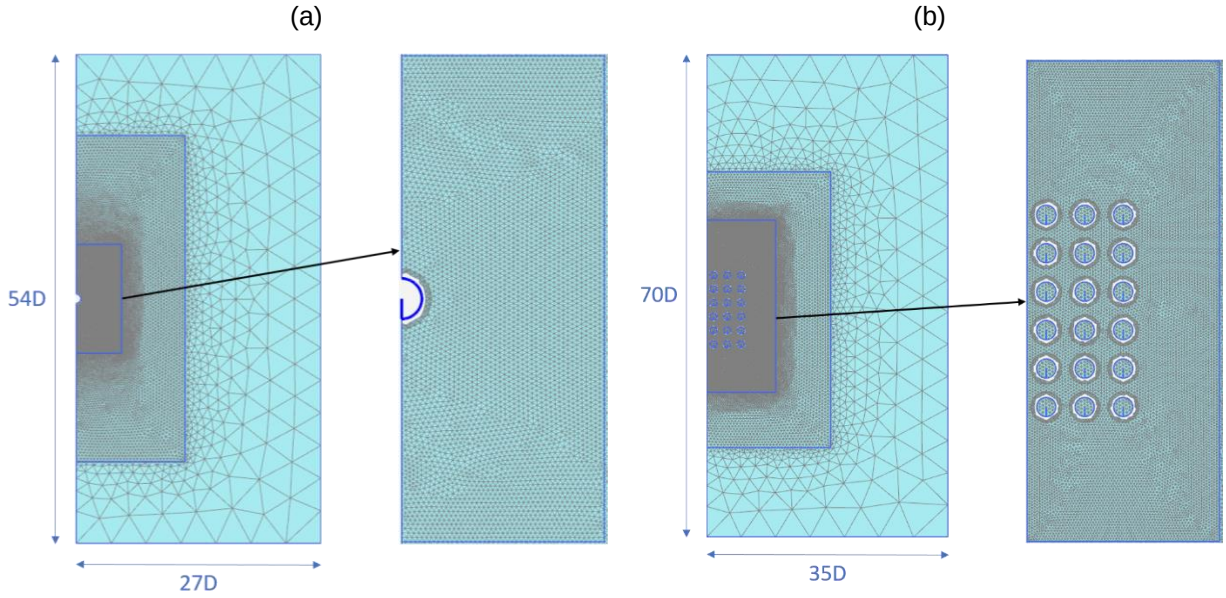

Fig. 2 Exemplar finite element meshes for (a) single pile (21239 elements), (b) 6×6 pile group (33959 elements).

Extraction of individual pile reactions

To extract the loads acting on individual group piles using this software, the prescribed pile displacements were applied to a single point at the end of a 'dummy' beam which was in turn fixed to the pile structure collinear with the direction of loading (see Fig. 3). Since the pile was modelled as a pipe with an internal cavity, the force generated by the prescribed displacement was fully transferred to the pipe structure through the dummy beam thereby allowing each individual pile force to be determined. The properties and thickness adopted for the steel pipe were also adopted for the dummy beam such that relative displacements between piles were less than 0.1%. In all cases, the sum of the individual pile reactions were identical to the FE output of the total reaction.

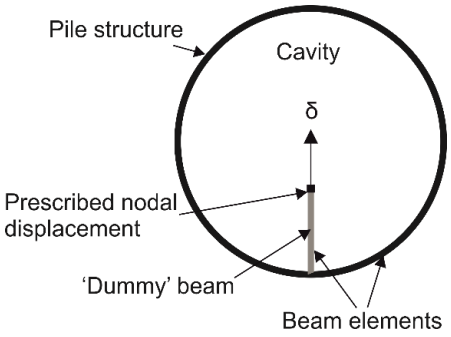

Fig. 3 Illustration of the dummy beam approach used for the extraction of individual group pile forces.

Verification

The results of the modelling are presented in terms of a dimensionless bearing capacity factor for a single pile, N_s, and pile group, N_g, as follows:

$$N_s = P_s / s_u D \quad (1)$$

$$N_g = P_g / s_u D n \quad (2)$$

where P_s and P_g are the total horizontal reaction per unit length for a single pile and an n pile group respectively obtained from the FE output. It can also be convenient to combine these parameters to produce a group efficiency factor, η_g:

$$\eta_g = N_g/N_s \quad (3)$$

Figure 4 presents predictions of N_s (Fig. 4(a)) and N_g for a 2×1 pile group (Fig. 4(b)) and a four−pile group (Fig. 4(c)), plotted as a function of normalised pile spacing, *s/D*. From Fig. 4(a), it can be seen that the present FE results are in very good agreement with rigorous plasticity solutions presented by Martin and Randolph (2006) and Randolph and Houlsby (1984) (all FE prediction lie within 1% of the Martin and Randolph (2006) solutions). Excellent agreement with solutions previously reported by Georgiadis et al. (2013b) and Zhao et al. (2017) can also be observed in Figs. 4(b) and Fig. 4(c) respectively.

(a)

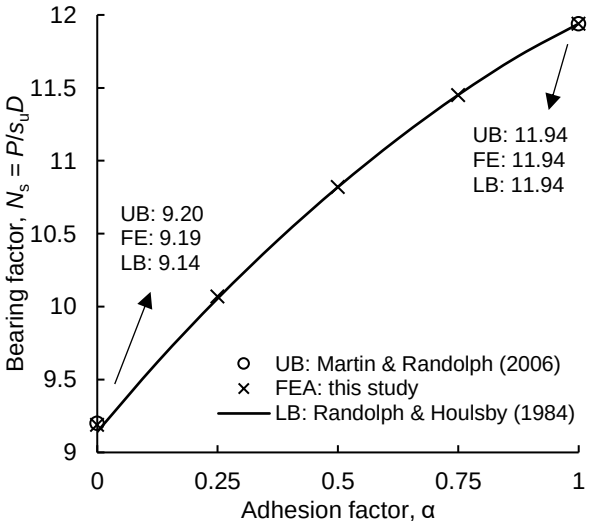

(b)

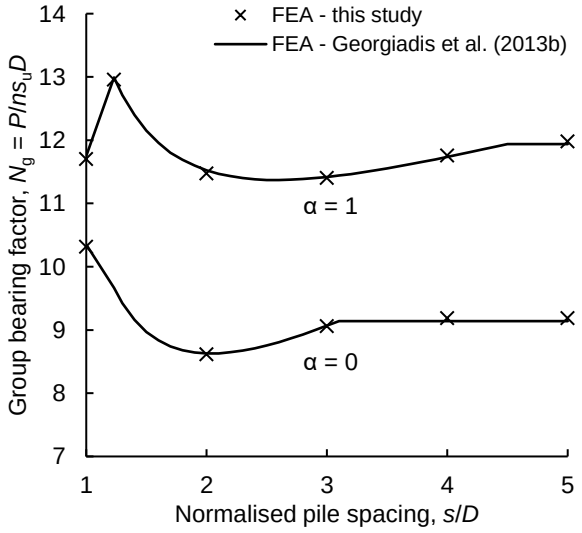

158 (c)

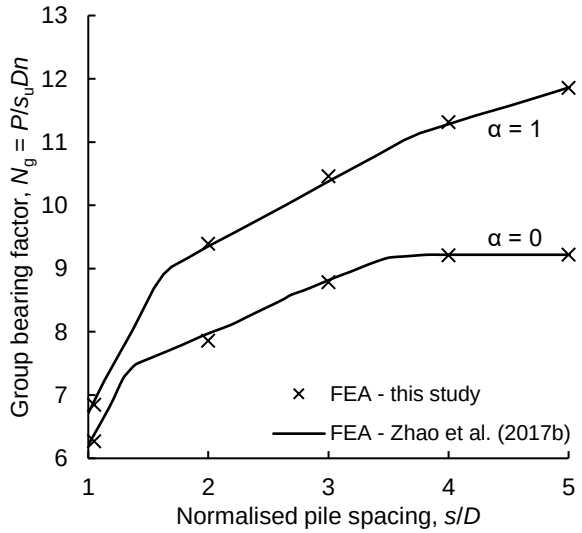

159

160 **Fig. 4** Validation of FE predictions using solutions previously documented in the literature: (a) single pile, (b)
161 two-pile group (n = 2; note in this instance loading is perpendicular to pile−to−pile axis), (c) four-pile group (n
162 = 4).

163 **SMALL GROUP RESULTS**

164 *Group bearing capacity and soil failure mechanisms*

165 For the sake of clarity, the problem definition from Fig. 1 has been applied to an n = 4 group in Fig.
166 5 showing all possible group shapes considered. The influence of group geometry on N_g is
167 explored in Fig. 6 for both a rough (α = 1; Fig. 6(a)) and smooth (α = 0; Fig. 6(b)) pile−soil
168 interface. Figure 6(a) shows that N_g is strongly influenced by the group shape, particularly for
169 closely spaced piles, where an increase in the number of pile rows, j, causes a reduction in N_g due
170 to overlapping shear zones between leading and trailing piles, henceforth referred to as pile
171 'shadowing effects'. For example, a steady reduction in N_g with decreasing s/D can be observed
172 for the 1×4 group where the relationship is approximately linear for $s/D \lesssim 3$ and slightly non-linear
173 in the region $3 \lesssim s/D \lesssim 6$ indicating gradual transitions between failure mechanisms.

174

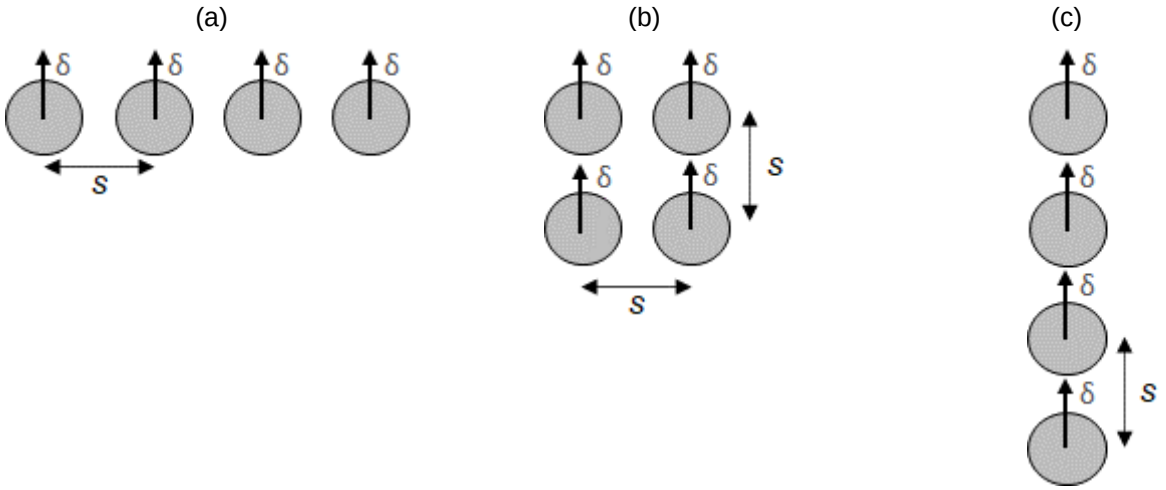

Fig. 5 Illustration of group shapes considered for the small pile group study: (a) 4×1, (b) 2×2, (c) 1×4.

In contrast, the influence of pile spacing on N_g is relatively insignificant for the conjugate 4×1 group in the region $s/D \gtrsim 2$. An interesting feature of the 4×1 data is that reductions in s/D below 2 causes N_g to reach a maximum value which exceeds that of an equivalent single pile ($\eta_g = 1.16$). While this behaviour may be unexpected, it has also been observed for laterally loaded two-pile groups (Georgiadis et al. 2013b). This capacity increase is due to a 'blocking' effect which causes soil between the piles to become trapped and move as a rigid body with the piles such that the group behaves as an equivalent non-circular pile of width $D + 3s$ (in this case; Georgiadis et al. 2013b). These findings are largely replicated in Fig. 6(b) for a smooth pile-soil interface except that values of η_g are slightly greater where a maximum of $\eta_g = 1.23$ is achieved for the 4×1 group. It can also be seen that group piles revert to individual single pile behaviour (i.e. $\eta_g = 1$) at higher pile spacings.

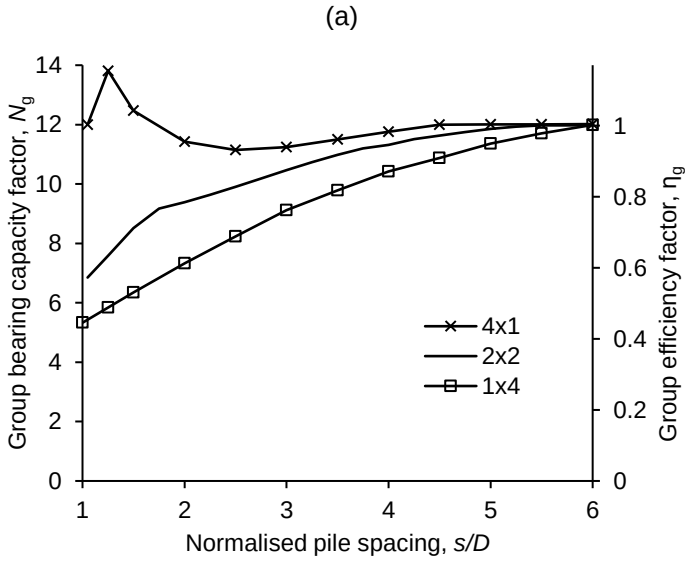

(b)

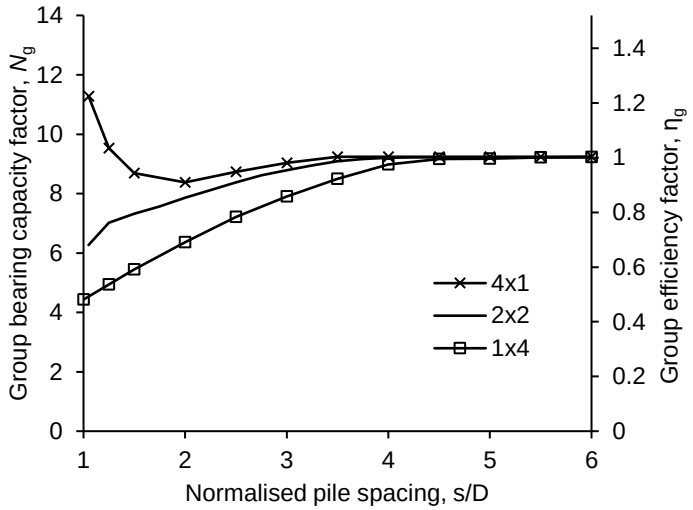

Fig. 6 FE predictions of the influence of group shape and pile spacing on the bearing capacity factor for n = 4 pile groups and for (a) rough (α = 1) and (b) smooth (α = 0) pile-soil interfaces.

To further explore the underlying causes of these trends, failure mechanisms for the 4×1 group are presented in Fig. 7 for values of *s/D* ranging between 1.05 and 5 and for α = 1 and 0. Figure 7 shows that the soil failure mechanisms correspond to single pile failure for *s/D* = 5, regardless of pile roughness. A reduction in *s*/*D* to 3 causes interactions to occur between piles where similar mechanisms are evident for both α = 1 and 0. For a rough interface, further reductions in *s/D* (to 1.25 and 1.05) reveal the blocking effect which causes sections of the soil to move with the piles, leading to the formation of a larger failure surface. However, this block failure mechanism does not fully form at the same spacings (*s/D* = 1.25 and 1.05) for the α = 0 case.

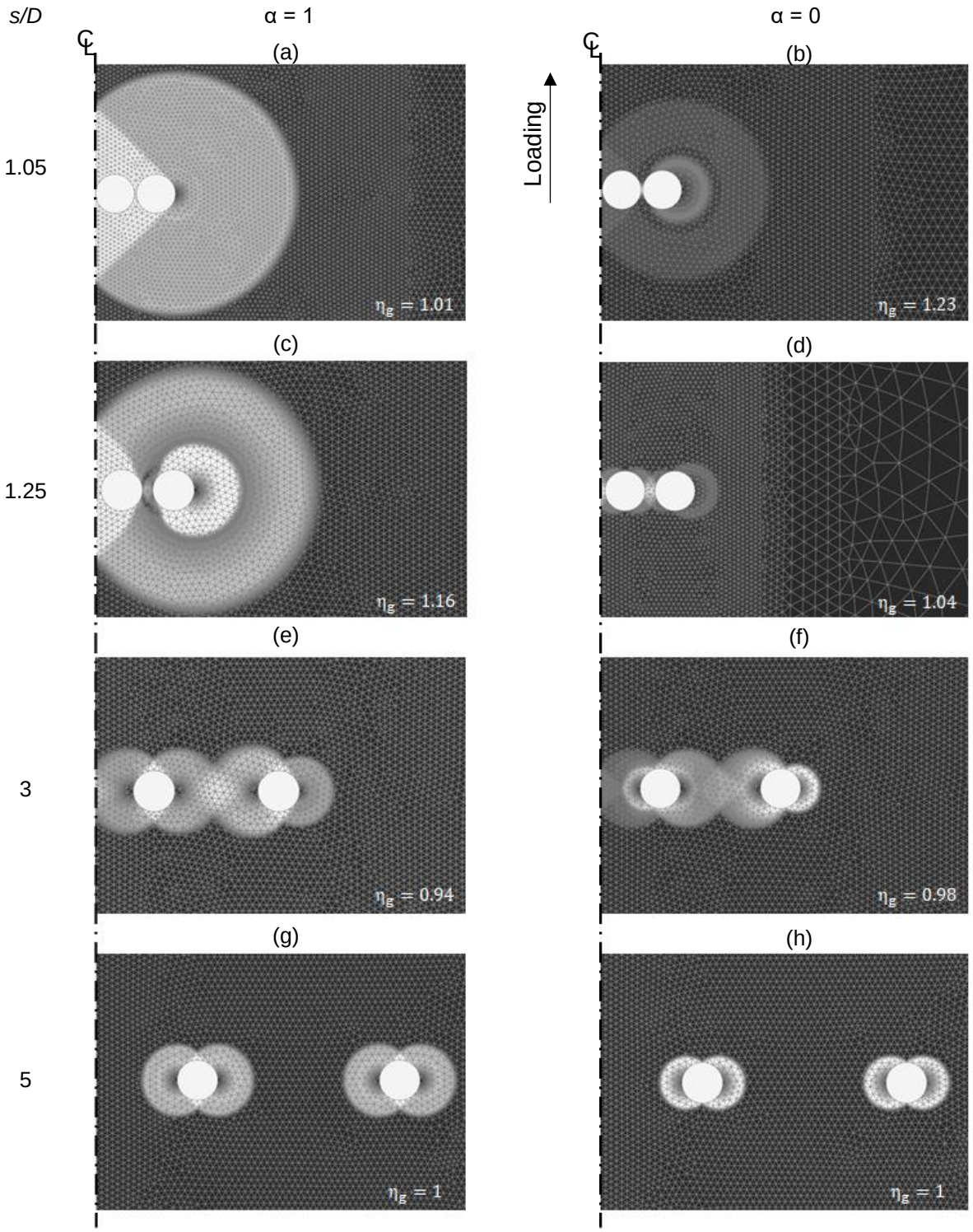

202 **Fig. 7** FE predictions of the influence of pile spacing and pile-soil interface roughness on soil failure
203 mechanisms using contours of incremental soil displacements for a 4×1 pile group shape (note only right-
204 hand side of mechanism shown due to symmetry).

205 Figure 8 shows the corresponding soil failure mechanisms for the conjugate 1×4 group. Only
206 mechanisms for α = 1 are shown in this figure due to similarity with the α = 0 mechanisms. In this
207 case, the transition between failure mechanisms is more subtle, reflecting the smoother

relationship observed in Fig. 6. Unlike the 4×1 group, interactions between piles occur even for *s/D* = 5 due to pile shadowing effects. While a reduction in *s/D* to 3 causes an amplification of these shadowing effects, a rigid body between soil and piles only occurs for values of *s/D* of 1.25 and 1.05. In this case, the mechanism resembles an equivalent 'wall' loaded parallel to its longest dimension. While these two mechanisms both correspond to this block 'wall' failure, a reduction in *s/D* from 1.25 to 1.05 causes further reductions in capacity due to a reduction in the equivalent wall length.

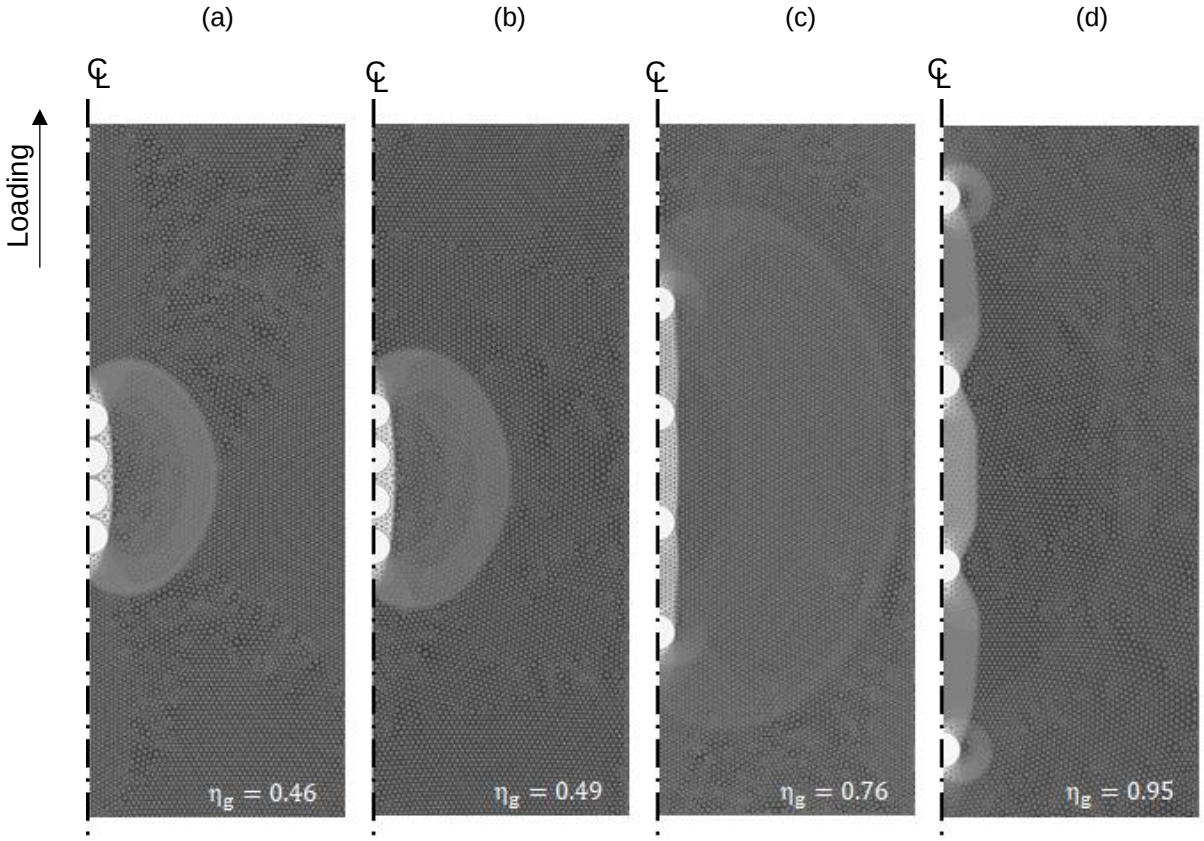

Fig. 8 FE predictions of the influence of pile spacing and pile-soil interface roughness on soil failure mechanisms using contours of incremental soil displacements for a 1×4 pile group shape (note only right-hand side of mechanism shown due to symmetry): (a) *s/D* = 1.05, (b) *s/D* = 1.25, (c) *s/D* = 3, (d) *s/D* = 5; rough pile-soil interface (α = 1).

Group load sharing

In Fig. 9, the variation in the bearing capacity factor for individual group piles (*N*) in the form of a percentage deviation from N_g is presented. The greatest deviation in the load-sharing within the

group occurs for the 1×4 group where outer piles experience loads 67% and 68% above the group average for α = 1 (Fig. 9(a)) and 0 (Fig. 9(b)) respectively. The shadowing effects observed in Fig. 8 cause the inner piles to generate less resistance as the intervening soil moves with the piles as a rigid body. In contrast, results from the 4×1 analyses show more uniform load sharing with a maximum deviations of 7% (α = 1) and 6% (α = 0). Note that all piles experience equal loads for a 2×2 group due to double symmetry. Surprisingly, there is a switch in the load sharing for 4×1 groups at small pile spacings, where the inner piles attract a greater proportion of the total load. This behaviour is explained by the failure mechanisms presented in Fig. 7 which shows a rigid 'false head' of soil moving with the inner piles whereas a 'flow-around' mechanism develops around the outer piles (e.g. at s/D = 1.25 for α = 1 and s/D = 1.05 for α = 0).

(a)

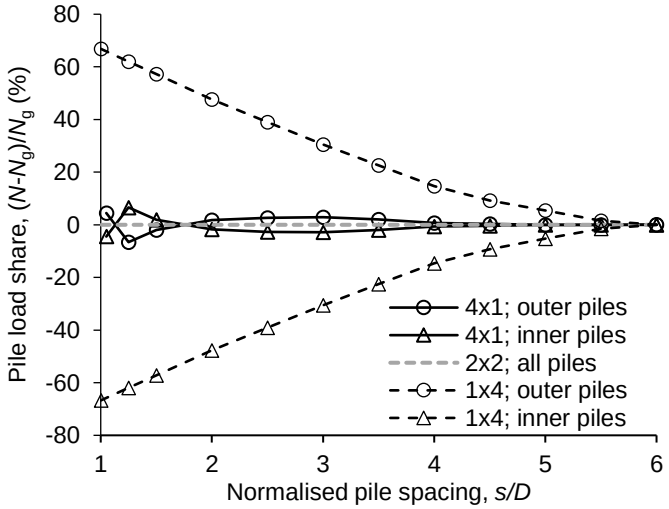

(b)

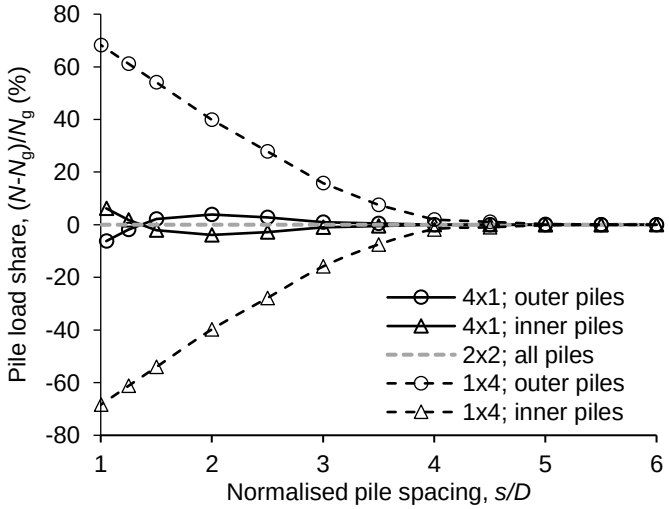

Fig. 9 FE predictions of the influence of group shape and pile spacing on the load-sharing within a 1×4 pile group for (a) rough (α = 1) and (b) smooth (α = 0) pile-soil interfaces.

LARGE PILE GROUP RESULTS

Group bearing capacity and soil failure mechanisms

FE predictions of N_g are plotted against the logarithm of the group geometry factor, *i/j*, in Fig. 10 for values of *s/D* of 2 and 4 and for both rough and smooth pile-soil interfaces. It can be observed that the relationship between N_g and *i/j* is highly non-linear. Taking the *s/D* = 2 results as an example, larger values of N_g are obtained for high values of *i/j* (i.e. 'wider' groups) where there appears to be a critical value of *i/j* beyond which any additional gains in N_g are insignificant. Reductions in *i/j* (i.e. 'narrower' groups) cause a significant drop in N_g, highlighting the greater influence of pile rows (*j*) on group interaction effects compared to pile columns (*i*). Interestingly, the minimum value of N_g corresponds to a 3×12 and 2×18 group geometry for α = 1 and 0, respectively, rather than the narrowest group (1×36). This is because the inclusion of additional pile rows promotes two competing mechanisms: (a) an increase in pile shadowing effects reduce group capacity and (b) the group behaves as an equivalent rigid 'wall' with an increasing length (≈ $D + (j - 1)\cdot s$) causing an increase in group capacity. It can also be seen that while α has a significant influence on N_g for wider groups, its influence is negligible for *i/j* ≤ 9/4. Though FE predictions of N_g for the *s/D* = 4 groups are notably greater than the corresponding *s/D* = 2 results, the resulting trends are remarkably similar. In this case, the minimum N_g corresponds to a 2×18 group regardless of the interface roughness whereas the value of *i/j* below which α has a negligible influence is 1 (square).

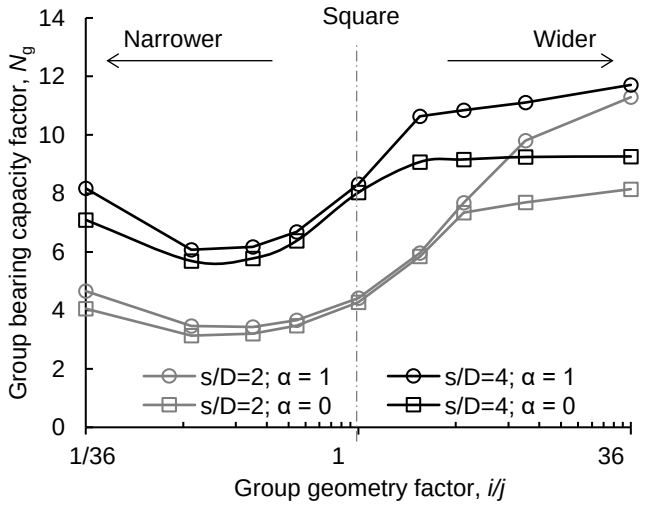

Fig. 10 FE predictions of the influence of group shape, pile spacing and pile-soil roughness on the bearing capacity factor for *n* = 36 pile groups.

These data are recast as group efficiency factors, η_g, in Fig. 11. Due to the apparent independence of α for narrow group geometries observed in Fig. 10, the α = 0 analyses exhibit greater efficiencies. These results therefore suggest that for large pile groups, significant increases in η_g can be realized for only a modest increase in the group geometry factor *i/j* compared to a standard square (*i/j* = 1) group shape. However, further increases in *i/j* eventually cause η_g to reach a plateau. It is noteworthy that even for an *n* = 36 group, a value of η_g = 1 can be achieved for *s/D* = 4 and α = 0 if a group geometry of *i/j* > 1 is adopted.

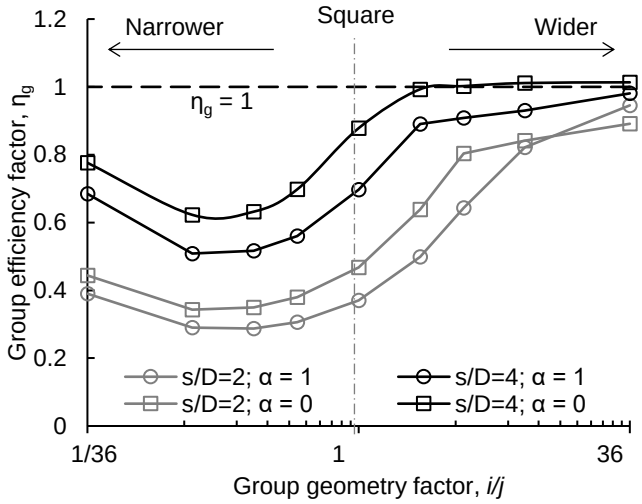

Fig. 11 FE predictions of the influence of group shape, pile spacing and pile-soil roughness on the group efficiency factor for *n* = 36 pile groups

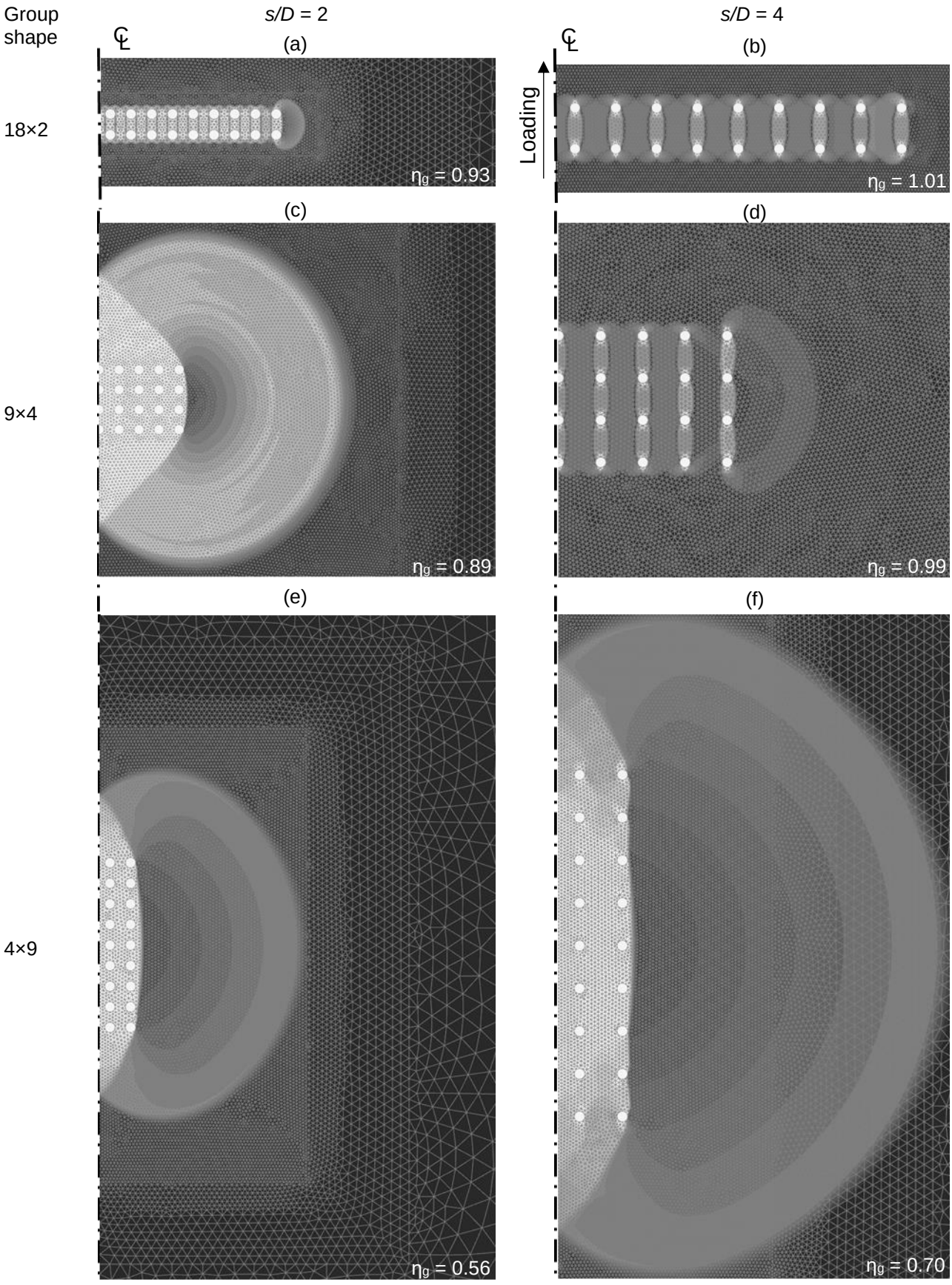
Group shape
s/D = 2
s/D = 4
(a)
(b)
(c)
(d)
(e)
(f)
18×2
9×4
4×9
Loading
ηg = 0.93
ηg = 1.01
ηg = 0.89
ηg = 0.99
ηg = 0.56
ηg = 0.70

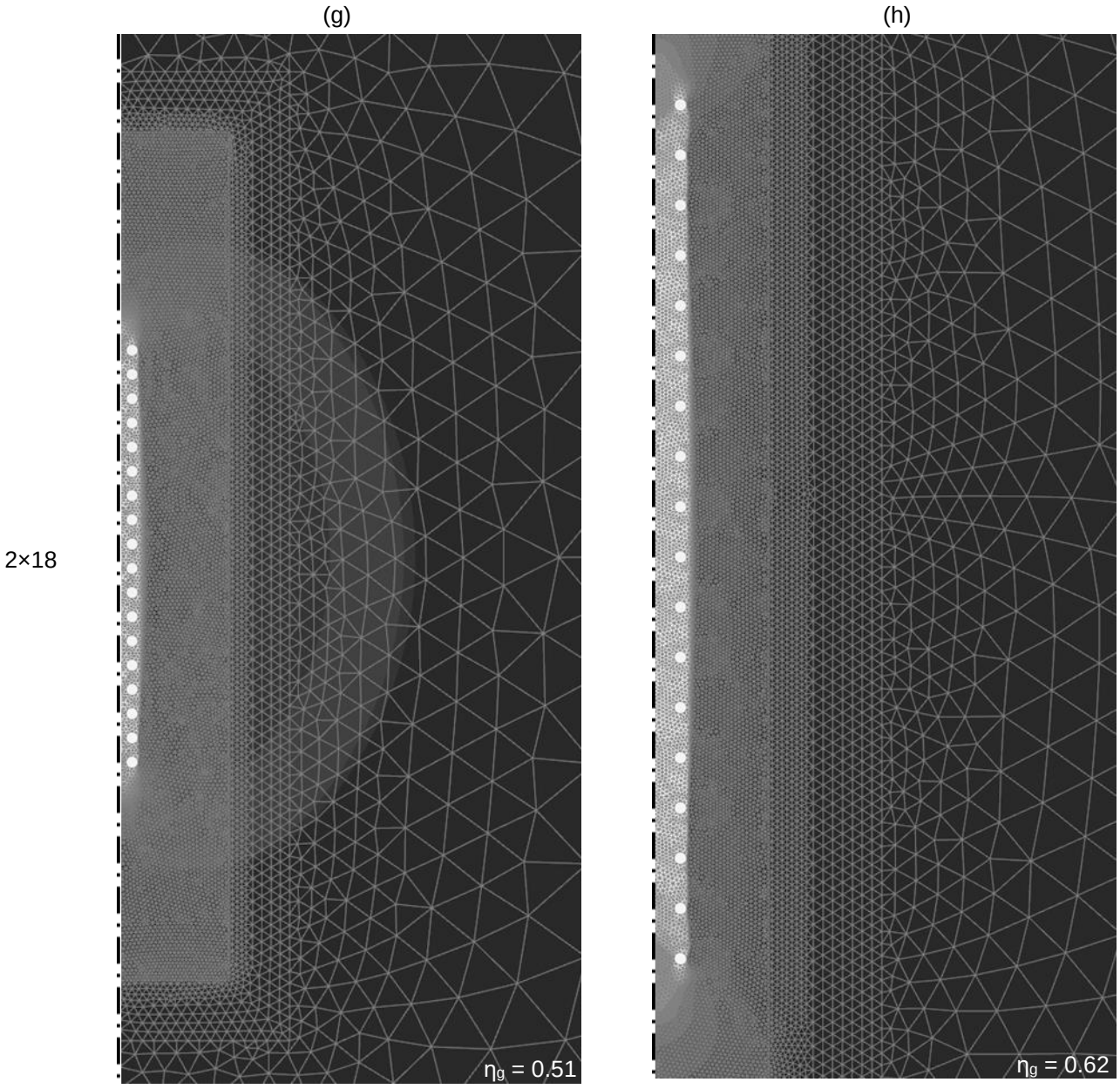

Fig. 12 FE predictions of the influence of pile spacing and group shape on soil failure mechanisms using contours of incremental soil displacements for a n = 36 pile groups (note only right-hand side of mechanism shown due to symmetry); rough pile-soil interface (α = 1).

To explore the source of the nonlinearity in these data, salient soil failure mechanisms are presented in Fig. 12 for s/D = 2 and 4 and for a rough pile-soil interface. The soil failure mechanisms for the 18×2 groups are complex, involving shadowing effects between the two pile rows and soil 'flow-around' between pile columns and towards the right-hand edge of the group (see Figs 12(a) and 12(b)). For the 9×4 group in Fig. 12(d), a similar mechanism is observed for s/D = 4, which explains the plateau in N_g and η_g observed at high values of i/j in Figs. 10 and 11, respectively. In contrast, there is a change in soil failure mechanism to block failure for s/D = 2

where the piles and intervening soil move as a rigid body, leading to a lower capacity, as shown in Fig. 12(c). This type of soil failure mechanism is applicable to lower values of *i/j* except that the composite pile-soil rigid body becomes narrower (see Figs 12(e)-12(h)). These block failure mechanisms also explain the independence of N_g on α for low values of *i/j* that were observed in Fig. 10 as shear failure planes exist predominantly in the soil mass rather than at the pile-soil interface.

Group load sharing

Given geometric and loading symmetry and the use of full tension interface conditions the load sharing within these rectangular groups are doubly symmetric; therefore, only quarter of the pile group is presented. Figure 13(a) and 13(b) plots the *p*-multipliers for individual group piles according to their position within a 36×1 and 1×36 group, respectively; the pile position (column and row) is numbered from the group edge inwards, in keeping with previous literature. These results are also presented in tabular form in Table 3. For the sake of conciseness, only results for $\alpha = 1$ are presented here given the similarity with the $\alpha = 0$ analyses. From Fig. 13(a), the group load sharing is uniform for both *s*/*D* = 2 and 4. This suggests that the group is behaving in a similar manner to an infinite pile row (Georgiadis *et al.* 2013c). For the conjugate 1×36 group, the load distribution is non-uniform where larger *p*-multipliers have been determined for piles closest to the group edge, as shown in Fig. 13(b). Interestingly, the outermost pile has similar *p*-multipliers for both values of *s*/*D* e.g. 0.93 and 1.0 for *s*/*D* = 2 and 4, respectively. Moving towards the centre of the group, *p*-multipliers decay rapidly and reach a steady value of 0.34 for s/D = 2 and 0.64 for s/D = 4 by pile row four. The greatest disparity between *p*-multipliers for the two pile spacings occurs at pile row 2. This indicates that for smaller pile spacings the leading row provides more effective 'shielding' of trailing piles.

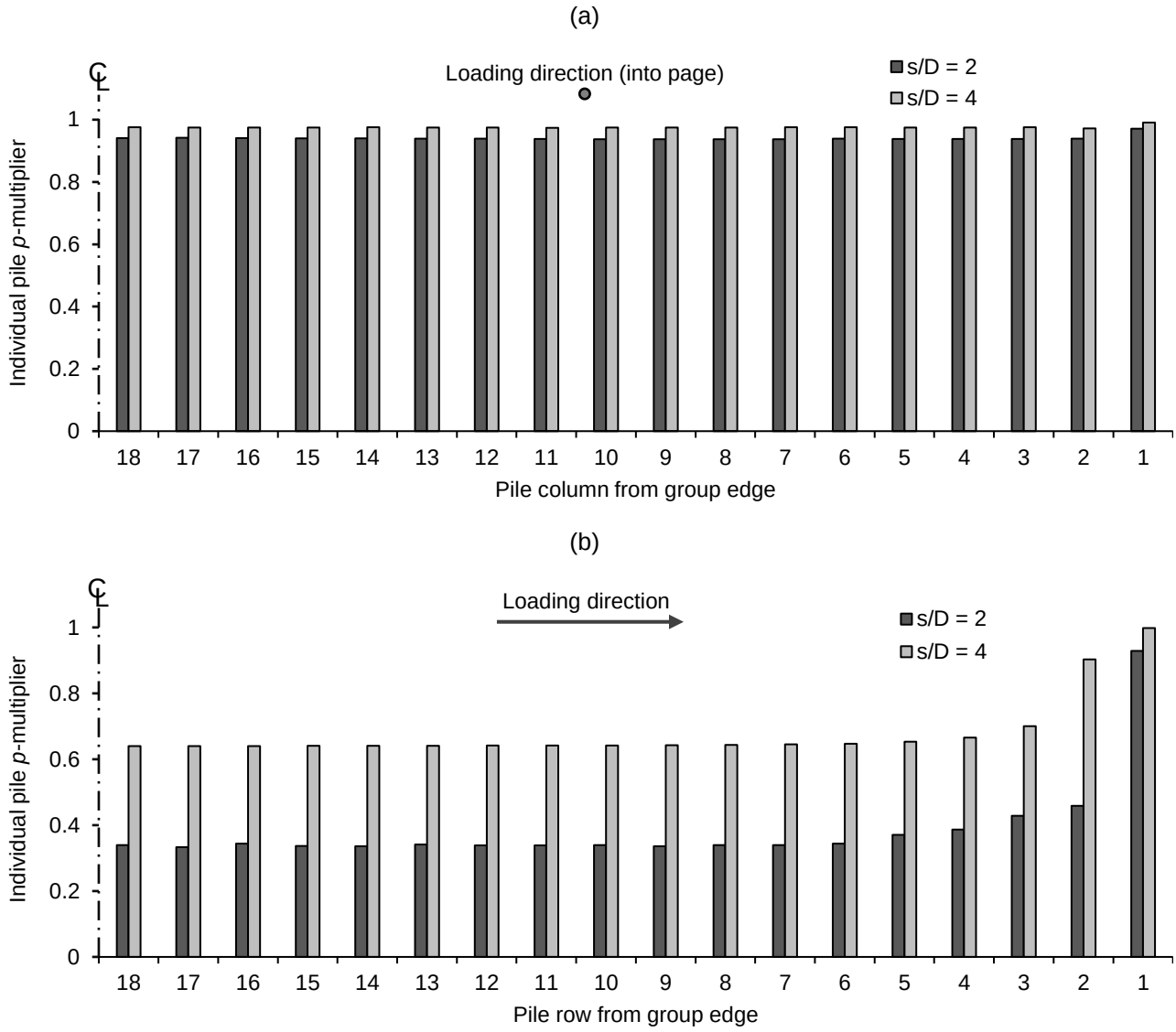

Fig. 13 FE predictions of the variation of individual *p*-multipliers within a (a) 36×1 and (b) 1×36 pile group for values of *s*/D of 2 and 4; rough pile-soil interface (α = 1).

Table 3 Tabulated FE predictions of the variation of individual *p*-multipliers within a 36×1 and 1×36 pile group for a rough pile-soil interface.

36×1 group			**1×36 group**		
Column number	***s/D* = 2**	***s/D* = 4**	**Row number**	***s/D* = 2**	***s/D* = 4**
1	0.97	0.99	1	0.93	1.00
2	0.94	0.97	2	0.46	0.90
3	0.94	0.98	3	0.43	0.70
4	0.94	0.98	4	0.39	0.67
5	0.94	0.98	5	0.37	0.65
≥6	0.94	0.98	≥6	0.34	0.64

The load sharing for the 18×2 group and its conjugate 2×18 group are presented in Fig. 14(a) and 14(b) respectively and are tabulated in Table 4. Results for the 18×2 group reveal constant *p*-multipliers for all piles apart from those in pile column 1. The uniformity of these results can be explained by the mechanisms presented in Fig. 12 which are identical within the group except for the outermost column, thus resulting in a slight deviation from the group average. Interestingly, for *s/D* = 2, this leads to a slight reduction in the *p*-multiplier for pile 1 which contradicts the traditional assumption that piles closer to the group edges always experience greater loads. There is also a more notable difference between the steady state *p*-multipliers compared to those obtained for the 36×1 group in Fig. 13(a) (0.82 and 0.92 for *s/D* = 2 and 4, respectively). For the 2×18 group in Fig. 14(b), it can again be observed that pile 1 experiences the largest *p*-multiplier where there is good agreement between the two pile spacings. By comparison to the 1×36 group presented in Fig. 13(b), these *p*-multipliers are notably lower and there is also a more gradual decay to the 'steady' *p*-multiplier which now appears to be dependent on *s/D*. For example, a constant *p*-multiplier is reached by pile row 4 for *s/D* = 2 compared to pile row 6 for *s/D* = 4.

(a)

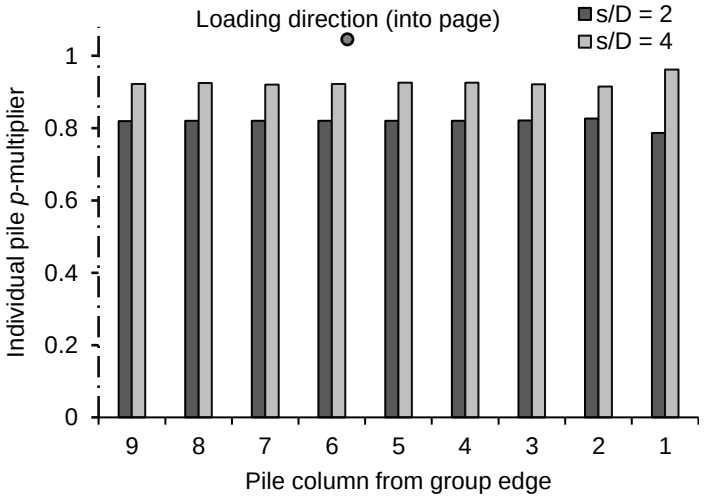

(b)

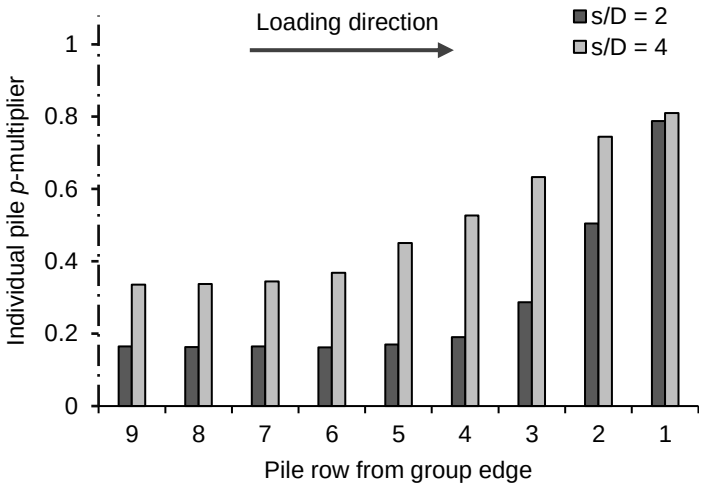

Fig. 14 FE predictions of the variation of individual *p*-multipliers within a (a) 18×2 and (b) 2×18 pile group for values of *s*/D of 2 and 4; rough pile-soil interface (α = 1).

Table 4 Tabulated FE predictions of the variation of individual *p*-multipliers within an 18×2 and 2×18 pile group for a rough pile-soil interface.

18×2 group			**2×18 group**		
Column number	***s/D* = 2**	***s/D* = 4**	**Row number**	***s/D* = 2**	***s/D* = 4**
1	0.79	0.96	1	0.79	0.81
2	0.83	0.92	2	0.50	0.74
3	0.82	0.92	3	0.29	0.63
4	0.82	0.93	4	0.19	0.53
5	0.82	0.93	5	0.17	0.45
≥6	0.82	0.92	≥6	0.16	0.37

Figure 15 shows the load sharing within the 9×4 and 4×9 groups which have also been tabulated in Tables 5 and 6 respectively. From Fig. 15(a), there is a notable variation in the *p*-multiplier across row 1 for *s/D* = 2 in a 9×4 group; while this phenomenon has been observed in centrifuge testing (Ilyas et al. 2004), it contradicts assumptions adopted in design guidelines commonly used by industry e.g. AASHTO (2012) and FEMA (2012). In contrast, the load distribution is notably more uniform for *s/D* = 4 with almost all piles experiencing equivalent loads (see Fig. 15(b))). A change in the group shape to 4×9 reveals more complex load sharing where variations occur across both group rows and columns. It is also noteworthy that the *p*-multiplier for the pile closest to the group

centre is 0.01 and 0.22 for *s/D* = 2 (Fig. 15(c)) and 4 (Fig. 15(d)), respectively. This suggests that for large rectangular pile groups, improved efficiency might be obtained by relocating central piles to mitigate group shadowing effects.

(a)

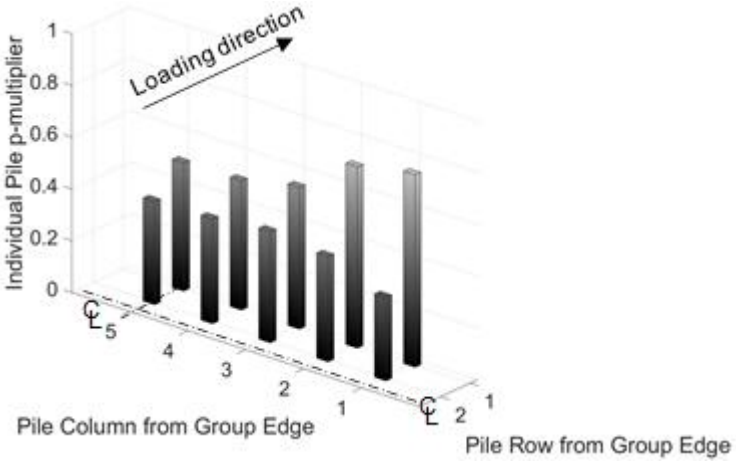

(b)

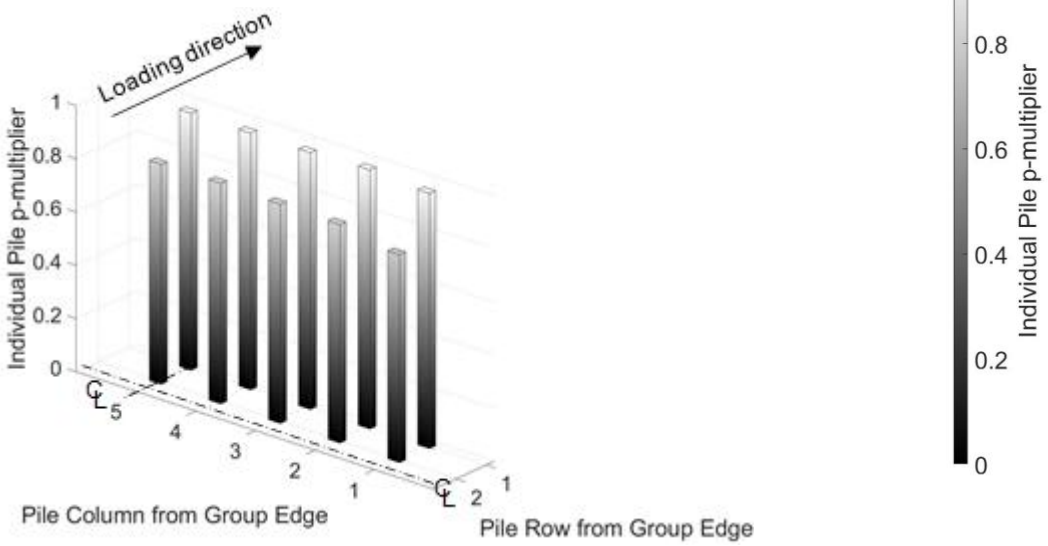

(c)

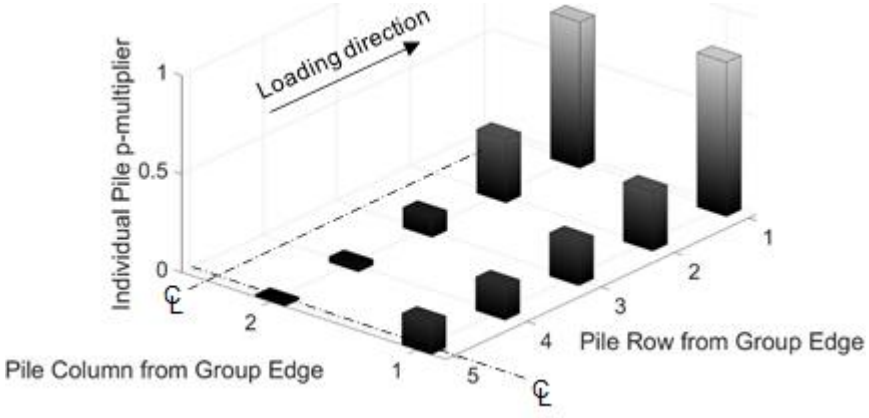

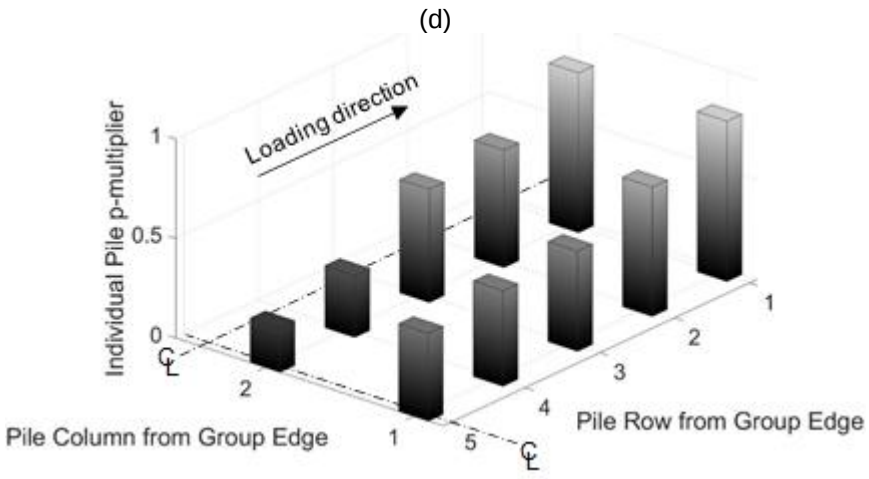

Fig. 15 FE predictions of the variation of individual *p*-multipliers for (a) 9×4, *s/D* = 2, (b) 9×4, *s/D* = 4, (c) 4×9, *s/D* = 2 and (d) 4×9, *s/D* = 4 groups; rough pile-soil interface (α = 1).

Table 5 Tabulated FE predictions of the variation of individual *p*-multipliers within a 9×4 pile group for a rough pile-soil interface.

		***s/D* = 2**		***s/D* = 4**	
Column number	**Row number:**	**1**	**2**	**1**	**2**
1		0.74	0.32	0.95	0.79
2		0.69	0.41	0.97	0.82
3		0.54	0.43	0.96	0.83
4		0.50	0.40	0.96	0.82
5		0.49	0.40	0.96	0.82

Table 6 Tabulated FE predictions of the variation of individual *p*-multipliers within a 4×9 pile group for a rough pile-soil interface.

		***s/D* = 2**		***s/D* = 4**	
Row number	**Column number:**	**1**	**2**	**1**	**2**
1		0.78	0.74	0.80	0.80
2		0.30	0.32	0.65	0.59
3		0.22	0.10	0.50	0.57
4		0.17	0.03	0.48	0.31
5		0.16	0.01	0.44	0.22

ANALYSIS AND DESIGN RECOMMENDATIONS

Influence of group rows and columns

The influence of the number of pile columns (*i*; perpendicular to direction of loading) on the relationship between N_g and *s/D* is presented in Figs. 16(a) – 16(d) for groups with *i* = 1 to 4 piles, respectively. Finite element results for alternative group sizes documented by Georgiadis et al. (2013a,b) and Sheil (2019) have also been plotted for comparison. For a given *i*, an increase in group size has a significant influence on N_g. This is particularly evident for groups with *i* = 2 columns where the group size controls the shape of the N_g – *s/D* relationship, as shown in Fig. 16(b). The pile-soil roughness also appears to have a greater influence on the small group sizes compared to the large *n* = 36 group.

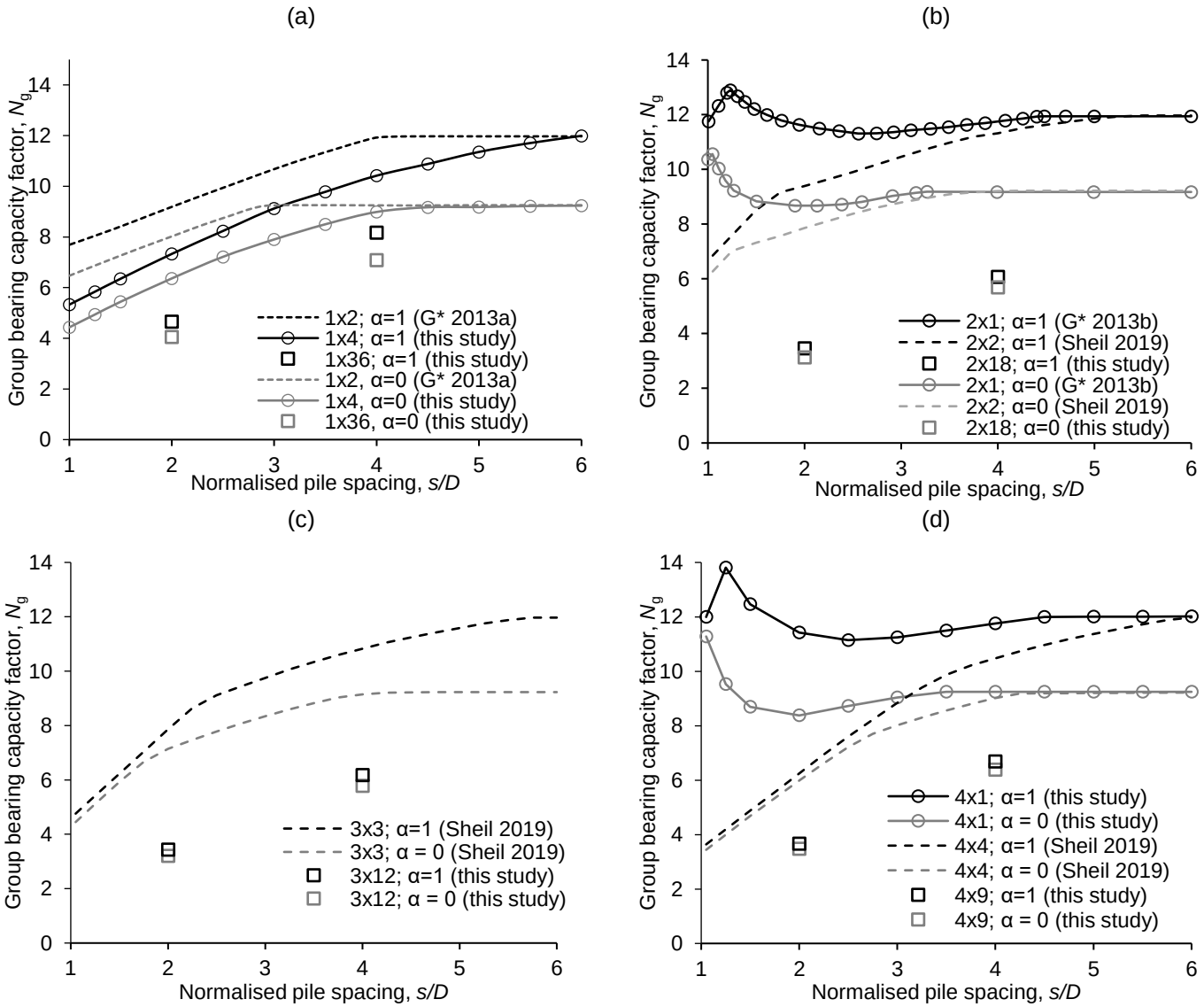

Fig. 16 FE predictions of the influence of group size on the group bearing capacity factor for a given number of pile columns, *i*, and for both rough and smooth pile-soil interfaces: (a) *i* = 1, (b) *i* = 2, (c) *i* = 3 and (d) *i* = 4. Note G* = Georgiadis et al.

The opposite is presented in Fig. 17 where now the influence of the number of group rows, *j*, on the N_g–*s/D* relationship is explored. For the same α, significantly improved agreement is obtained between groups of different sizes. The only exception is the *j* = 4 results presented in Fig. 17(d) where there is some disparity between results for low values of *s/D*. Nevertheless, these results show that N_g is almost entirely dominated by the number of pile rows *j*. It follows that for large non-standard rectangular groups, the value of N_g can be determined using existing solutions proposed for smaller group sizes provided the same value of *j* is maintained. To this end, pile group design equations previously documented in the literature are discriminated by *j* in Table 7. Predictions determined by a selection of these methods are superimposed on the plots in Fig. 17 where excellent agreement with the numerical output can be observed.

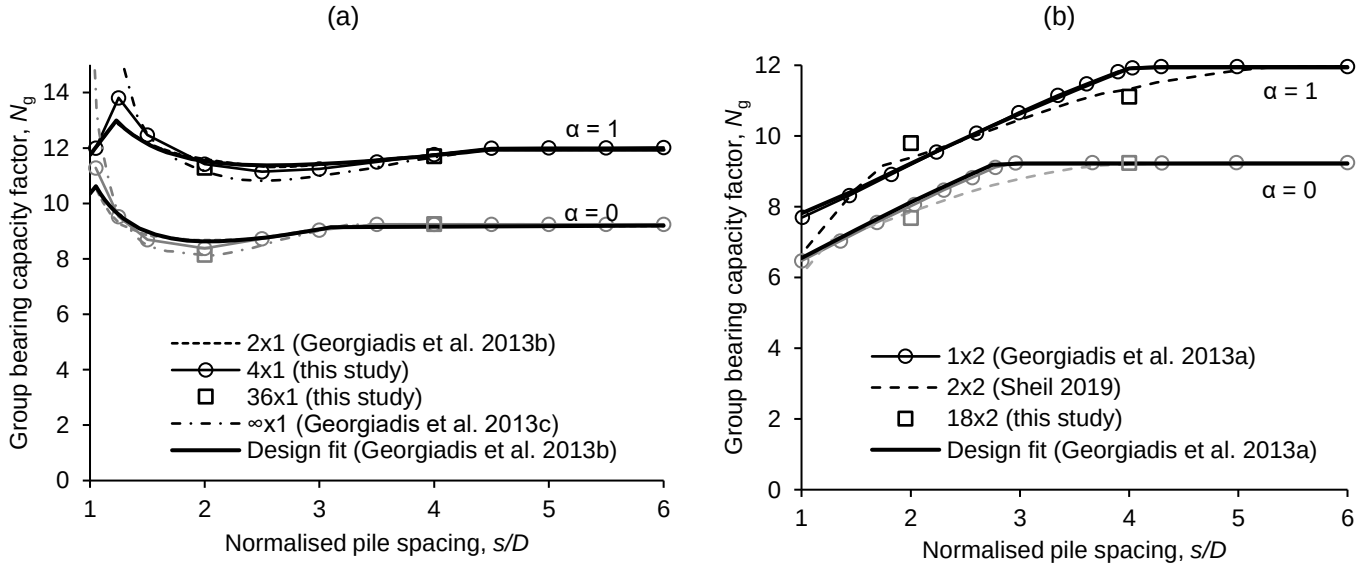

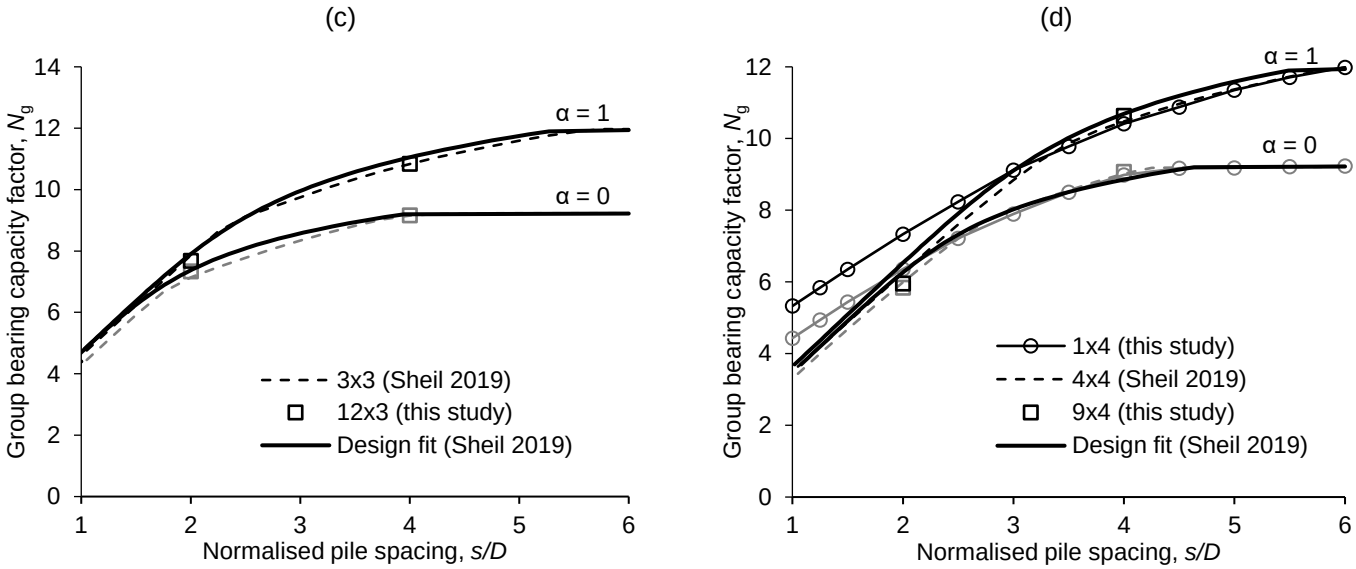

385 **Fig. 17** FE predictions of the influence of group size on the group bearing capacity factor for a given number
386 of pile rows, *j*, and for both rough and smooth pile-soil interfaces: (a) *j* = 1, (b) *j* = 2, (c) *j* = 3 and (d) *j* = 4.

387

388 **Table 7** Existing design methods reported in the literature for the determination of the 'deep-condition'
389 ultimate soil resistance for pile groups with *j* rows.

Number of group rows, *j*	Design method	Basis for design method
1	Equations (14) – (19) in Georgiadis et al. (2013b)	2×1
2	Equations (10) – (22) in Georgiadis et al. (2013a) Equations (35) – (25) in Zhao et al. (2017b) Equations (1) – (6) in Sheil (2019)	1×2 2×2 2×2
3	Equations (1) – (6) in Sheil (2019)	3×3
4	Equations (1) – (6) in Sheil (2019)	4×4
5	Equations (1) – (6) in Sheil (2019)	5×5
6, 9, 12, 18, 36	Figures 10 and 11 in this study	6×6, 4×9, 3×12, 2×18, 1×36 (respectively)

390

391

392 *P-multipliers: comparison to existing design guidelines*

393 Figure 18 presents design charts for the determination of *p*-multipliers depending on their row-wise
394 location within the group for both rough and smooth interface. The results presented earlier in Figs.

13 – 15 demonstrated that the load sharing across a given row is not necessarily uniform. This contrasts with existing design guidelines which assume a constant *p*-multiplier for a given row. Present *p*-multiplier predictions have therefore been averaged for each row while the minimum and maximum values for a given row are denoted using error bars. The results are plotted in Fig. 18 as a function of the group geometry factor (*i/j*). Also superimposed on the figure are values recommended by the AASHTO (2012) and FEMA (2012) design guidelines (see Tables 8 and 9, respectively). Linear interpolation and extrapolation has been used to determine *p*-multipliers for values of *s/D* of 4 and 2, respectively, when using the AASHTO (2012) guidelines.

It can be observed that the *p*-multipliers within the group are highly dependent on group geometry, pile-soil interface roughness and pile spacing. For a small group (n = 4), the group geometry factor appears to dominate the resulting *p*-multiplier. Even though a reduction in α and/or increase in *s/D* results in a slight increase in the resulting *p*-multiplier, the trends with group shape remain largely unchanged. It is also notable that the influence of the geometry factor on the *p*-multiplier is highly dependent on the pile's row-wise location. For example, the role of *i/j* is suppressed for row 1 because all piles are edge piles, regardless of the geometry. In contrast, for row 2, the piles for i/j = 1 are edge piles whereas the pile for i/j = 1/4 is now a central pile; this leads to very different *p*-multipliers.

While these findings also apply to the results obtained for the large group, the trends are much more uniform owing to the greater number of piles which leads to a smoother transition between group shapes. It can also be seen that minimum *p*-multipliers for large pile groups correspond to near-square group shapes. It should be noted that while the design guidelines do not capture the complex dependence of the *p*-multipliers on group geometry, predictions compare well to the minimum *p*-multiplier for a given group size. In particular, the AASHTO (2012) design guidelines provide a very good lower bound estimate of the data.

Two approaches exist for the inclusion of these predictions within existing design methods using: (a) the group bearing capacity factor, representing an average for the group (Figure 17 and Table 7), and (b) *p*-multipliers for each individual group pile (Figure 18). Present predictions of N_g for the

group may be incorporated within existing design methods capable of describing the overall load-displacement of the group which take the overall capacity reduction as input, such as those proposed by Comodromos and Pitilakis (2005) and Comodromos and Papadopoulou (2012, 2013). Alternatively, group piles may be treated individually using the *p*-multiplier corresponding to their position within the group (e.g. AASHTO (2012) and FEMA (2012)) to modify existing *p-y* formulations e.g. Brown and Shie (1991), Kallehave et al. (2012), Dash et al. (2017), Zhang and Anderson (2017).

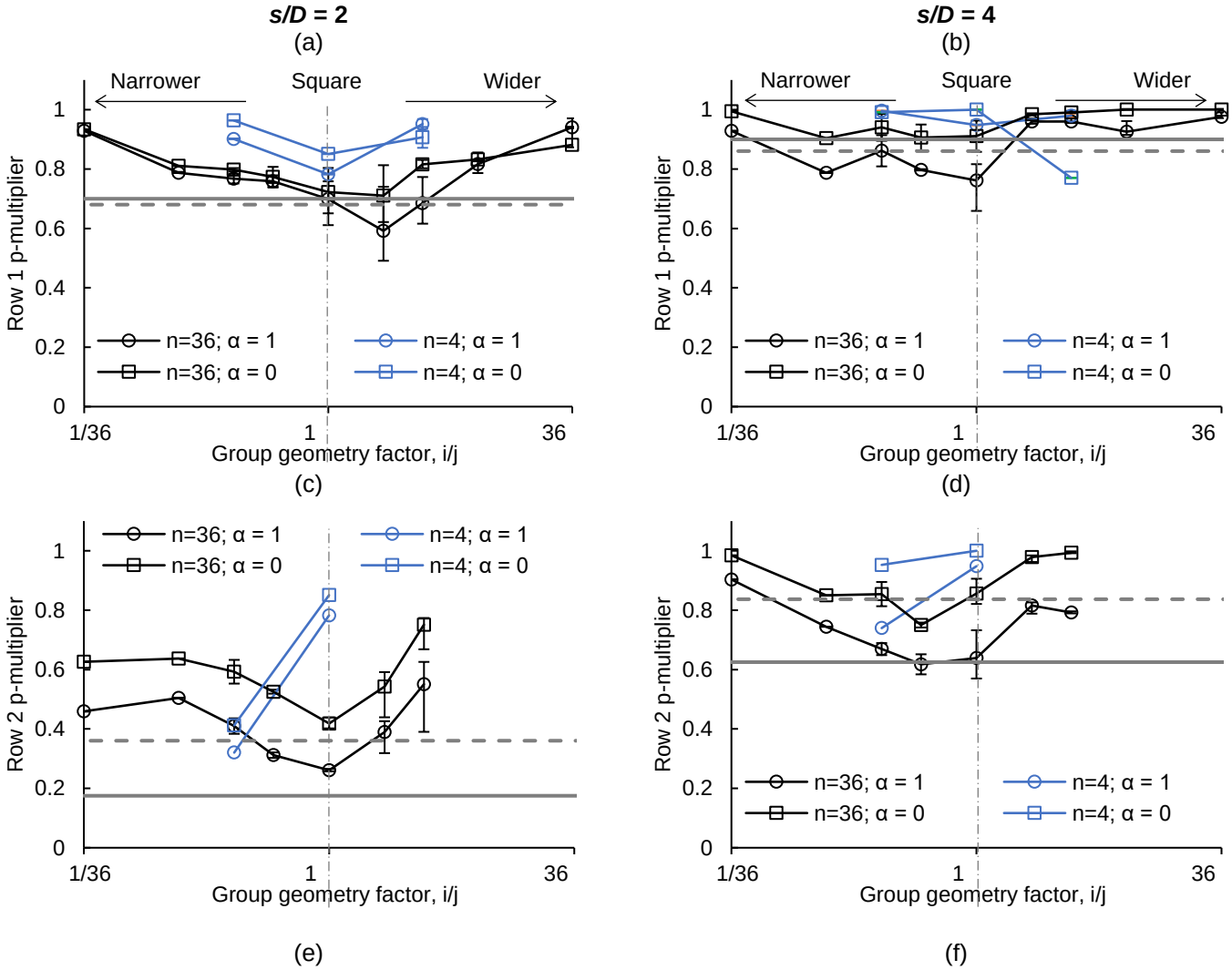

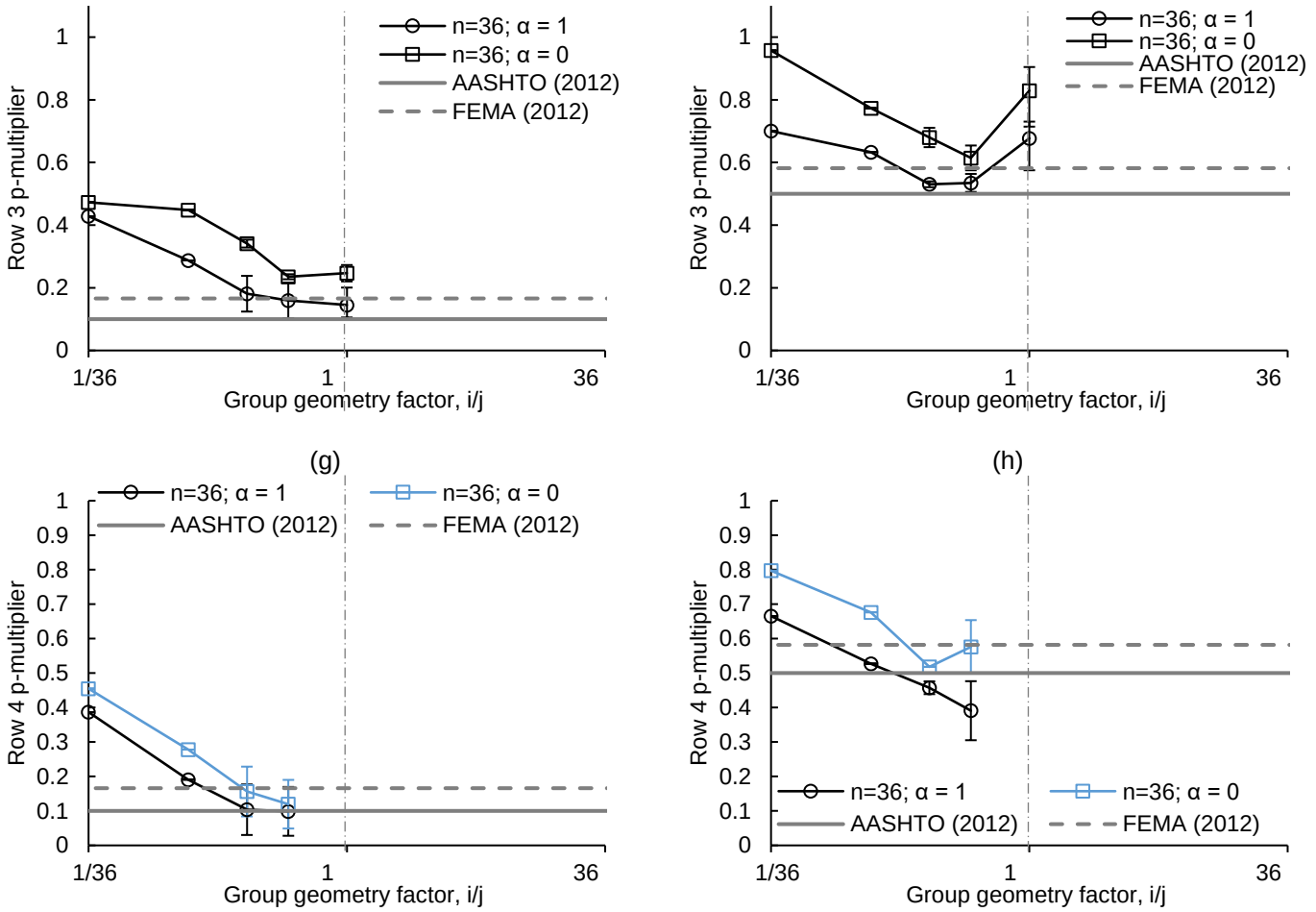

Fig. 18 Comparison between FE predictions of *p*-multipliers (averaged for a given row) and predictions determined using the AASHTO (2012) and FEMA (2012) design guidelines: (a) row 1, *s/D* = 2; (b) row 1, *s/D* = 4; (c) row 2, *s/D* = 2; (d) row 2, *s/D* = 4; (e) row 3, *s/D* = 2; (f) row 3, *s/D* = 4; (g) row 4, *s/D* = 2; (h) row 4, *s/D* = 4. Error bars denote the range in the *p*-multipliers across the row.

Table 8 Definition of *p*-multipliers using the AASHTO (2012) design guidelines.

Row number	**Normalised pile spacing, *s/D***	
	3	**5**
1	0.8	1.0
2	0.4	0.85
≥3	0.3	0.7

Table 9 Definition of *p*-multipliers using the FEMA (2012) design guidelines.

Row number	***p*-multiplier**
1	$0.26 \ln(s/D) + 0.5 \leq 1.0$

2	$0.52 \ln(s/D) \leq 1.0$
≥3	$0.60 \ln(s/D) - 0.25 \leq 1.0$

436

437 **LIMITATIONS OF MODELLING**

438 The main limitation of the modelling described in this paper is the omission of depth effects. While
439 pile interaction effects are constant beyond a critical depth, FE results reported by Georgiadis
440 (2014) show that pile interaction varies closer to the ground surface. In addition, pile flexibility may
441 allow differential pile displacements to develop at some depth along the length of the piles, leading
442 to slight alterations in group interaction effects (Sheil and McCabe 2016). However, minor changes
443 to pile spacing arising from realistic pile differential displacements are not expected to have an
444 appreciable influence on the results presented in this paper.

445 The results presented in this paper were performed using a small-strain FE formulation. In practice,
446 the displacements required to achieve failure of the pile group may be such that a large
447 deformation analysis may be required. Full tension pile-soil interface conditions (i.e. no gapping)
448 were imposed to study deep flow-around failure mechanisms and are unlikely to apply to near-
449 surface wedge-type failure mechanisms. This study therefore investigates only the maximum
450 resistance that may develop along the length of the piles and not the distribution of the lateral
451 resistance with depth. Clearly further research on depth effects are warranted for the development
452 and implementation of a self-contained design method for the overall integrated response of a pile
453 group in practice. Nevertheless, this paper provides an improved understanding, and rigorous
454 predictions, of the role of group shape on the ‘deep-condition’ soil limiting pressure which should
455 be an underpinning element for the development of more complete three-dimensional solutions for
456 laterally loaded pile groups.

457

458 **CONCLUSIONS**

459 This paper has described a finite element study of the behaviour of a pile group embedded in
460 undrained clay soil subjected to lateral loading. Plain strain conditions have been assumed such

461 that the ‘deep condition’ soil limiting pressure is investigated. The primary aim of the study was to
462 explore the influence of pile group shape effects on the soil limiting pressure considering both a
463 small (four piles) and large (36 piles) group. Additional parameters considered in the modelling
464 include pile spacing and pile-soil interface roughness. The main conclusions from the study are as
465 follows:

466 (a) For both small and large pile groups, the group capacity was shown to be strongly
467 influenced by the group shape. For a given group size, an increase in the number of pile
468 rows (parallel to direction of loading) was shown to reduce capacity due to ‘shadowing’
469 effects. Conversely, an increase in the number of pile columns (perpendicular to direction of
470 loading) was found to increase capacity due to a ‘blocking’ effect which causes the soil
471 between the piles to move as a rigid body effectively behaving as a larger non-circular pile
472 for closely spaced piles. The minimum capacity for the large pile group was not obtained for
473 the narrowest group but for an intermediate configuration due to two competing
474 mechanisms: while an increase in shadowing effects within the group caused a reduction in
475 capacity, the group behaves as an equivalent ‘wall’ with an increasing length causing an
476 increase in capacity.
477 (b) The results suggest that for large pile groups, significant increases in capacity efficiency
478 can be realized for only a modest increase in the group geometry factor *i/j* compared to
479 standard square (*i/j* = 1) configurations. However, further increases in *i/j* eventually causes
480 the efficiency to reach a plateau.
481 (c) In contrast with assumptions adopted by existing design guidelines, the present results
482 show that the load distribution within the group is highly non-uniform, varying across both
483 the group rows as well as columns, and is dependent on group size and shape and pile-soil
484 roughness. Minimum *p*-multipliers were typically obtained for near-square groups.
485 However, predictions determined using the FEMA (2012) and particularly the AASHTO
486 (2012) design guidelines were shown to provide very good lower bound approximations to
487 the finite element results.

(d) The influence of the geometry factor on the *p*-multiplier was also shown to be highly dependent on the pile's row-wise location, particularly for small pile groups. For example, the role of the group shape was suppressed for row 1 because all piles are edge piles, regardless of the geometry. In contrast, for row 2, the piles for a 2×2 group are also edge piles whereas the pile for a 1×4 group is now a central pile; this leads to very different *p*-multipliers.

(e) The results show that the group bearing capacity factor is almost entirely dominated by the number of rows in the group such that existing design equations presented elsewhere in the literature can be repurposed for larger groups with the same number of pile rows. A framework was proposed for future implementations of the present results through the development of a 'library' of design methods. Specifically, two approaches were identified: (i) capacity reduction of the *entire group* using numerical predictions of the bearing capacity factor and (ii) capacity reduction of *individual piles* within the group using *p*-multipliers corresponding to the location of the pile within the group.

REFERENCES

AASHTO, L. (2012) AASHTO LRFD bridge design specifications.

Brown, D.A., Morrison, C. and Reese, L.C. 1988. Lateral load behaviour of pile group in sand. *Journal of Geotechnical Engineering*, *114*(11), 1261−1276.

Brown, D.A. and Shie, C.F. 1991. Some numerical experiments with a three dimensional finite element model of a laterally loaded pile. *Computers and Geotechnics*, *12*(2), 149−162.

Chandrasekaran, S.S., Boominathan, A. and Dodagoudar, G.R. 2010. Group interaction effects on laterally loaded piles in clay. *Journal of Geotechnical and Geoenvironmental Engineering*, *136*(4), 573-582.

Comodromos, E.M and Pitilakis K. 2005. Response Evaluation of Horizontally Loaded Fixed-Head Pile Groups using 3-D Nonlinear Analysis, *International Journal for Numerical and Analytical Methods in Geomechanics*, 29(6), 597-625.

Comodromos E.M. and Papadopoulou M.C. 2012. On the response prediction of laterally loaded pile groups in clayey soils. *Géotechnique*, 62(4), 329–339.

Comodromos E.M., Papadopoulou M.C. 2013. Explicit extension of the p-y method to pile groups in cohesive soils, *Computers & Geotechnics*, 47, 28-41.

Dash, S., Rouholamin, M., Lombardi, D. and Bhattacharya, S., 2017. A practical method for construction of py curves for liquefiable soils. *Soil Dynamics and Earthquake Engineering*, *97*, 478-481.

Fayyazi, M.S., Taiebat, M. and Liam Finn, W.D. 2014. Group reduction factors for analysis of laterally loaded pile groups. *Canadian Geotechnical Journal*, *51*(7), 758-769.

FEMA, 2012. "Foundation analysis and design", FEMA P−751, Washington, DC.

Georgiadis, K., 2014. Variation of limiting lateral soil pressure with depth for pile rows in clay. *Computers and Geotechnics*, *62*, pp.164−174.

527 Georgiadis, K., Sloan, S.W. and Lyamin, A.V., 2013a. Effect of loading direction on the ultimate
528 lateral soil pressure of two piles in clay. *Géotechnique*, *63*(13), 1170.
529 Georgiadis, K., Sloan, S.W. and Lyamin, A.V., 2013b. Ultimate lateral pressure of two
530 side−by−side piles in clay. *Géotechnique*, *63*(9), 733.
531 Georgiadis, K., Sloan, S.W. and Lyamin, A.V., 2013c. Undrained limiting lateral soil pressure on a
532 row of piles. *Computers and Geotechnics*, 54, 175−184.
533 Kallehave, D., Thilsted, C.L. and Liingaard, M.A., 2012, January. Modification of the API py
534 formulation of initial stiffness of sand. In *Offshore site investigation and geotechnics:*
535 *integrated technologies-present and future*. Society of Underwater Technology.
536 Ilyas, T., Leung, C.F., Chow, Y.K. and Budi, S.S. 2004 Centrifuge model study of laterally loaded
537 pile groups in clay. *Journal of Geotechnical and Geoenvironmental Engineering*, *130*(3), 274-
538 283.
539 Martin, C.M. and Randolph, M.F., 2006. Upper-bound analysis of lateral pile capacity in cohesive
540 soil. *Géotechnique*, *56*(2), 141-145.
541 Matlock, H., 1970. Correlations for design of laterally loaded piles in soft clay. Offshore technology
542 in civil engineering's hall of fame papers from the early years, 77−94.
543 McCabe, B.A. and Sheil, B.B., 2015. Pile group settlement estimation: suitability of nonlinear
544 interaction factors. *International Journal of Geomechanics*, *15*(3), 04014056.
545 Murff, J.D., Wagner, D.A. and Randolph, M.F., 1989. Pipe penetration in cohesive soil.
546 *Géotechnique*, *39*(2), 213-229.
547 Murff, J.D. and Hamilton, J.M., 1993. P−ultimate for undrained analysis of laterally loaded
548 piles. *Journal of Geotechnical Engineering*, *119*(1), 91−107.
549 Randolph, M.F. and Houlsby, G.T., 1984. The limiting pressure on a circular pile loaded laterally in
550 cohesive soil. *Geotechnique*, *34*(4), 613−623.
551 Rollins, K.M., Olsen, K.G., Jensen, D.H., Garrett, B.H., Olsen, R.J. and Egbert, J.J., 2006. Pile
552 spacing effects on lateral pile group behaviour: Analysis. *Journal of Geotechnical and*
553 *Geoenvironmental Engineering*, 132(10), 1272−1283.
554 Sheil, B.B. and McCabe, B.A., 2014. A finite element–based approach for predictions of rigid pile
555 group stiffness efficiency in clays. *Acta Geotechnica*, *9*(3), 469−484.
556 Sheil, B.B. and McCabe, B.A., 2015. Numerical modelling of pile foundation angular distortion.
557 Soils and Foundations, 55(3), 614−625.
558 Sheil, B.B. and McCabe, B.A., 2016. An analytical approach for the prediction of single pile and
559 pile group behaviour in clay. *Computers and Geotechnics*, *75*, pp.145-158.
560 Sheil, B.B. and McCabe, B.A., 2017. Biaxial loading of offshore monopiles: numerical
561 modeling. *International Journal of Geomechanics*, *17*(2), p.04016050.
562 Sheil, B.B., McCabe, B.A., Comodromos, E.M. and Lehane, B.M., 2018. Pile groups under axial
563 loading: an appraisal of simplified non-linear prediction models. *Géotechnique*, 1-15.
564 Sheil, B.B., 2020. Lateral limiting pressure on square pile groups in undrained soil. *Géotechnique*,
565 DOI: 10.1680/jgeot.18.P.118.
566 Yang, Z. and Jeremić, B., 2002. Numerical analysis of pile behaviour under lateral loads in layered
567 elastic–plastic soils. *International Journal for Numerical and Analytical Methods in*
568 *Geomechanics*, *26*(14), 1385-1406.
569 Zhang, Y. and Andersen, K.H., 2017. Scaling of lateral pile py response in clay from laboratory
570 stress-strain curves. *Marine Structures*, *53*, pp.124-135.
571 Zhao, Z., Kouretzis, G., Sloan, S. and Gao, Y., 2017a. Ultimate lateral resistance of tripod pile
572 foundation in clay. *Computers and Geotechnics*, *92*, 220−228.
573 Zhao, Z., Li, D., Zhang, F. and Qiu, Y., 2017b. Ultimate lateral bearing capacity of tetrapod jacket
574 foundation in clay. *Computers and Geotechnics*, *84*, 164−173.
575